

High magnetic anisotropy and magnon excitations in single crystals of the double spin chain compound $\text{PbMn}_2\text{Ni}_6\text{Te}_3\text{O}_{18}$

I. Panneer Muthuselvam ^{1,2,*}, K. Saranya,² Florian Büscher ³, Dirk Wulferding ⁴, Peter Lemmens,^{3,†} Wei-tin Chen,⁵ and R. Sankar⁵

¹Department of Physics (MMV), Banaras Hindu University, Varanasi-221005, Uttar Pradesh, India

²Department of Physics, School of Basic and Applied Sciences, Central University of Tamil Nadu, Thiruvavur 610005, Tamil Nadu, India

³Institute of Condensed Matter Physics and Laboratory for Emergent Nanometrology (LENA),

TU-Braunschweig, 38106 Braunschweig, Germany

⁴Center for Correlated Electron Systems, Institute for Basic Science and Department of Physics and Astronomy, Seoul National University, Seoul 08826, Republic of Korea

⁵Center for Condensed Matter Sciences, National Taiwan University, Taipei 10617, Taiwan and Institute of Physics, Academia Sinica, Nankang, Taipei 11529, Taiwan



(Received 16 July 2020; revised 30 October 2020; accepted 4 January 2021; published 1 February 2021)

We have successfully grown single crystals of $\text{PbMn}_2\text{Ni}_6\text{Te}_3\text{O}_{18}$ and present a comprehensive study of their magnetic, thermodynamic, and Raman spectroscopic properties. $\text{PbMn}_2\text{Ni}_6\text{Te}_3\text{O}_{18}$ consists of a planar network of pairwise rotated NiO_6 dimers coupled by corners. Similarities to Ni_3TeO_6 exist, which forms honeycomb layers. The magnetic susceptibility χ and heat capacity C_p data reveal an antiferromagnetic phase transition around 84 K, which is evidently hysteretic on warming and cooling between 94 and 40 K with a loop width of about 1.83 ± 0.41 K; thus the transition appears to be of first order. χ is anisotropic, with larger values for in-plane fields over the entire measured temperature range. Raman spectroscopy has been employed to investigate the lattice and magnetic excitations of the $\text{PbMn}_2\text{Ni}_6\text{Te}_3\text{O}_{18}$ from 5 to 300 K. Besides an anharmonic phonon behavior, i.e., a decay into acoustic phonons, we find a coupling to the spin system at $T_N = 84$ K, as well as weak anomalies at $T^* \approx 200$ K. This second characteristic temperature gives evidence for an instability of the coupled spin/lattice system, as here the phonon linewidths and intensities evidence similar behavior as at $T_N = 84$ K. Furthermore, magnetic Raman scattering at 240 cm^{-1} is used to estimate an exchange coupling of $J = -86$ K in general agreement with the Curie-Weiss temperature.

DOI: [10.1103/PhysRevB.103.064401](https://doi.org/10.1103/PhysRevB.103.064401)

I. INTRODUCTION

Low-dimensional magnetic systems based on an integer, spin-1 antiferromagnetic (AF) Heisenberg exchange have attracted enormous interest for many years after the Haldane conjecture was established [1,2]. This topological argument predicated that quasi-one-dimensional (1D) $S = 1$ Heisenberg antiferromagnets exhibit a spin gap between the singlet ground state and the first excited triplet state. An ideal Haldane chain system is difficult to find experimentally; even if a spin gap is found in a quasi-1D integer spin chain system, it is not sufficient to claim the existence of a Haldane ground state, not to mention that an unavoidable, weak interchain coupling produces a long-range ordering at sufficiently low temperatures. A Haldane gap has been suggested for the 1D $S = 1$ CsNiCl_3 spin chain system [2]. Nevertheless, antiferromagnetic (AF) long-range order below $T_N \sim 4.9$ K has also been found as a result of weak interchain coupling [3,4].

From the previously studied Haldane spin chain candidates, the series REBaNiO_5 (RE is rare earth Yb to Dy) has

drawn considerable interest because of the coexistence of a Haldane gap and long-range magnetic order (from $T_N \sim 8.8$ K to $T_N \sim 65$ K) for the different magnetic rare earth members [5–7]. The combination of mixed spins and a quasi-one-dimensional arrangement of $S = 1$ could be a valuable origin of exotic magnetic ground states. It will therefore certainly be a fruitful playground for further discoveries.

$\text{PbMn}_2\text{Ni}_6\text{Te}_3\text{O}_{18}$ crystallizes in a hexagonal structure with the space group $P6_3/m$. Its crystal structure is shown in Fig. 1(a), where the NiO_6 and TeO_6 octahedra form a double chain structure running along the c axis, shown in Fig. 1(c) [8]. Thus, this double chain can be considered as a 1D chain system consisting of Ni^{2+} ($S = 1$) ions. Meanwhile, Mn^{2+} ions are trigonal-prismatic coordinated by O^{2-} [Fig. 1(b)]. In addition, this compound has a triangle-based array of chains in the ab plane, reflecting the hexagonal symmetry, which may induce geometrical frustration in the interchain magnetic interaction. Therefore, $\text{PbMn}_2\text{Ni}_6\text{Te}_3\text{O}_{18}$ might potentially evidence some unique magnetic behavior.

The magnetic properties of polycrystalline $\text{PbMn}_2\text{Ni}_6\text{Te}_3\text{O}_{18}$ have been reported previously [9]. Here, we have prepared single crystals and systematically studied their magnetic and thermal properties. We find that $\text{PbMn}_2\text{Ni}_6\text{Te}_3\text{O}_{18}$ exhibits a strongly anisotropic behavior. In

*ipmphysics@gmail.com

†p.lemmens@tu-bs.de

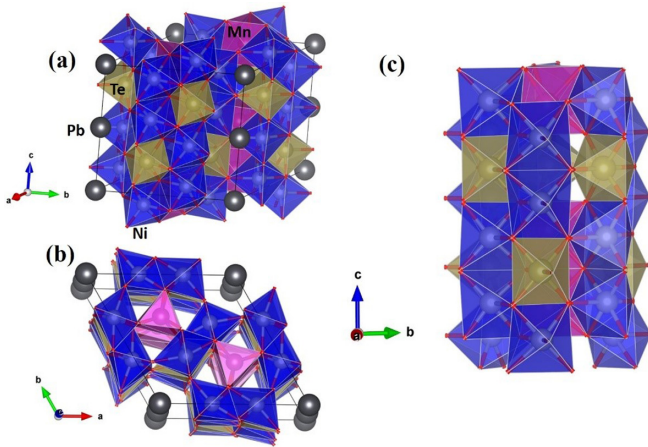


FIG. 1. (a) Crystal structure of $\text{PbMn}_2\text{Ni}_6\text{Te}_3\text{O}_{18}$. (b) The crystal structure along the c axis showing the arrangement of the atoms in the ab plane. (c) Chains along the c axis.

addition, using Raman spectroscopy we found evidence for further instabilities in the temperature range between 5 and 300 K.

II. EXPERIMENTAL DETAILS

Single crystals of $\text{PbMn}_2\text{Ni}_6\text{Te}_3\text{O}_{18}$ are grown by the flux method. High-purity NiO (99.995%), TeO_2 , MnCO_3 and PbO were loaded into an alumina crucible in a typical molar ratio of 5:5:3:1 [8]. The mixed powder was initially calcinated to 650°C for 10 h and then heated and kept at 850°C for 24 h, before cooling to 700°C at 1.5°C/h . Afterwards, the sample was cooled to room temperature. The sample was then removed from the furnace and dark-green shiny crystals were obtained. In order to examine the chemical composition, electron probe microanalysis (EPMA) was used which confirms the chemical composition. The EPMA analysis is carried out at seven selected positions on the single crystal. After averaging values from each spot and normalizing them to Pb we obtain a ratio of Pb : Mn : Ni : Te : O = 1 : 2.01 : 5.99 : 3.03 : 17.97. This ratio is in good agreement with the target stoichiometry. The consistency of the normalized values of O content suggests that oxygen vacancies do not play any role in the present compound.

Synchrotron x-ray diffraction patterns (SXR) were collected with 20 keV beam energy at room temperature at beamline BL01C2, Taiwan Light Source, National Synchrotron Radiation Research Center, Taiwan. The sample was packed in a 0.1-mm-diameter borosilicate capillary, which was kept spinning during data collection. The patterns were recorded on a MAR345 image plate and converted with GSAS 2 software. The Rietveld refinement was carried out with the Bruker TOPAS software package. Dc and ac magnetization (M) measurements were performed using a Vibrating sample magnetometer - Superconducting Quantum Interference Device (Quantum Design). The heat capacity (C_p) of the sample was measured down to 2 K using a Quantum Design physical properties measurement system (PPMS). Raman scattering experiments were performed using a Raman

microscope (Horiba LabRAM HR 800) with a solid state laser as an excitation source and a wavelength of $\lambda = 532.5$ nm. Samples were cooled on a cold finger of a microscope cryostat in vacuum. A notch filter in the spectrometer allowed measurements with Raman shifts larger than 55 cm^{-1} .

III. RESULTS AND DISCUSSION

Figure 2(a) shows the excellent crystallinity with the sharp peaks of the $\text{PbMn}_2\text{Ni}_6\text{Te}_3\text{O}_{18}$ single crystal, which can be indexed as $(h\ 00)$ reflections in accordance with the hexagonal space group $P6_3/m$. The room temperature SXR patterns of the crushed powder sample are illustrated in Fig. 2(b). The Rietveld refinement was carried out to the space group $P6_3/m$, revealing a good coincidence, as shown in Fig. 2(b). A 3.83% minority phase of NiO is also detected from this sample. The systematic temperature dependence of SXR evidences no structural changes down to 116 K. The unit cell parameters are estimated from SXR by Rietveld analysis at different selected temperatures, as shown in Figs. 2(c) and 2(d). With decreasing temperature, the lattice parameters decrease monotonically. The atomic and lattice parameters refined at 300 K are in agreement with Refs. [8,9] and are given in Table I.

Figure 3 shows the temperature dependences of the zero-field-cooled (ZFC) and field-cooled (FC) magnetic susceptibility, $\chi = M/H$, for fields along the crystallographic c axis (black curve), perpendicular to the c axis (red curve), and for a powder sample of $\text{PbMn}_2\text{Ni}_6\text{Te}_3\text{O}_{18}$ (green curve). It is interesting to note that for fields perpendicular to the c axis the value of χ is larger than for fields along the c axis at every measured temperature. χ increases monotonically with decreasing temperature and forms a broad maximum at around 92 K, which is characteristic for low-dimensional systems. After a sharp drop at 84 K, χ decreases gradually down to 7 K for fields along the c axis followed by an upturn below 7 K. For fields perpendicular to the c direction, as well as in the powder sample, χ increases with decreasing temperature after passing through a minimum at 60 and 20 K, respectively. The low-temperature upturn in χ is related to broken chains and the presence of a small number of paramagnetic impurities. This signature is observed in many low-dimensional magnetic materials [10]. Below T_N , the decrease of χ for H along c towards low temperatures demonstrates that the magnetic spins are aligned along the c axis in the three-dimensional (3D) antiferromagnetic (AFM) ordered state, which agrees well with previously reported data from neutron diffraction measurements, suggesting a magnetic easy axis along the c axis.

The derivatives of $\chi(T)$ show a prominent peak located at 84.5 K, indicating 3D AFM long-range order. The observed T_N is close to the previously reported $T_N = 86$ K for a polycrystalline sample. As shown in the lower inset of Fig. 3, interestingly, the expanded view of ZFC and FC curves shows a thermal hysteresis behavior near the magnetic transition in the temperature range between 94 and 40 K for fields parallel and perpendicular to the c axis, as well as for the pulverized sample, suggesting a first order contribution to the magnetic phase transition. The observed average hysteresis loop width

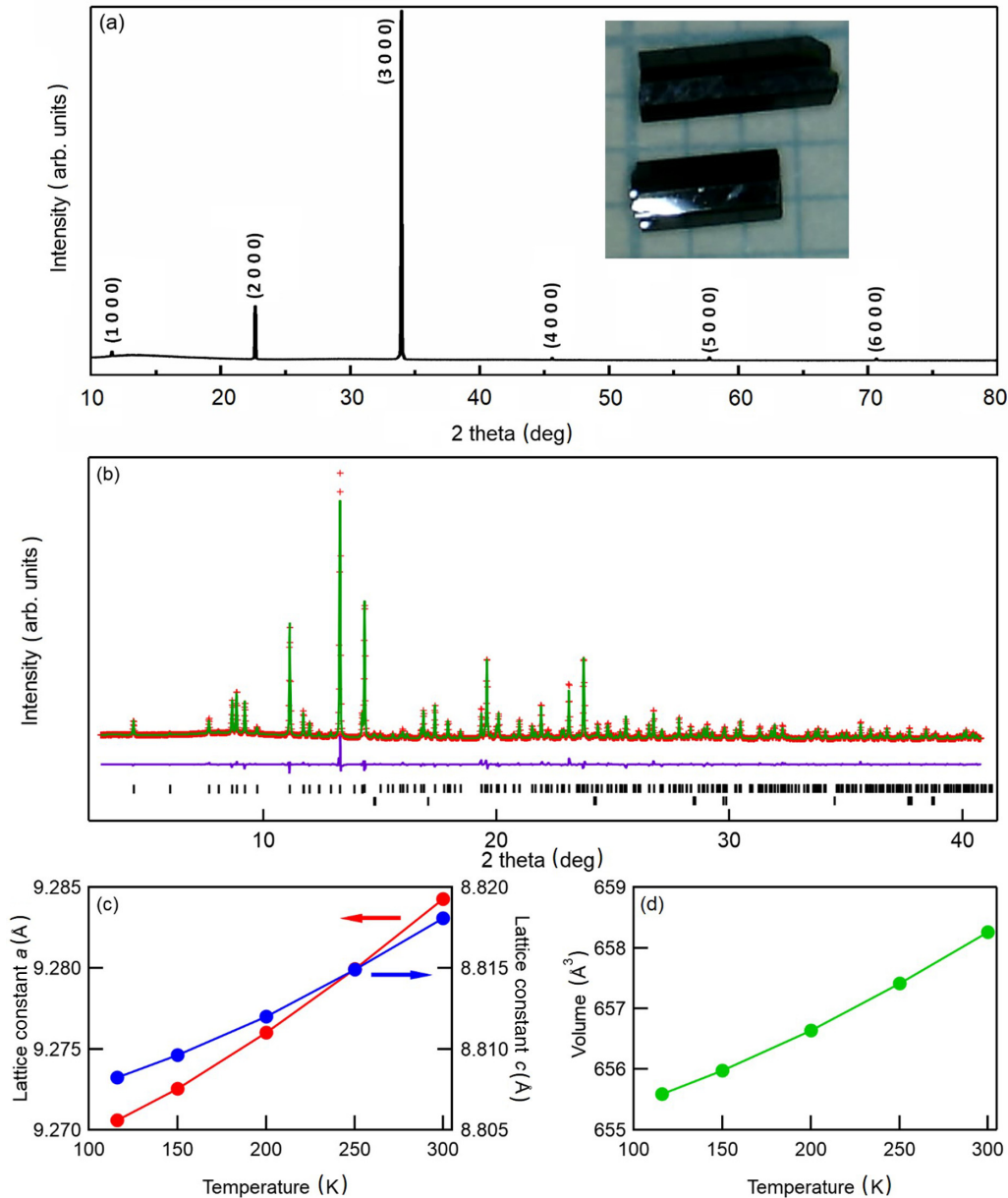


FIG. 2. (a) Single crystal x-ray diffraction pattern of $\text{PbMn}_2\text{Ni}_6\text{Te}_3\text{O}_{18}$. Inset shows typical single crystal images of $\text{PbMn}_2\text{Ni}_6\text{Te}_3\text{O}_{18}$. The appearance of a broad bumplike feature between 10° and 20° is due to the x-ray sample holder which is usually amorphous in nature. (b) The synchrotron x-ray diffraction patterns of crushed single crystals at 300 K. The red symbols represent the experimental data; the solid green line is the two-phase Rietveld refinement of $\text{PbMn}_2\text{Ni}_6\text{Te}_3\text{O}_{18}$ (space group $P6_3/m$) and (minor) NiO (space group $Fm-3m$). The short black vertical bars indicate the Bragg peak positions of both phases. The purple solid curve represents the difference between the experimental and calculated diffraction patterns. (c), (d) The temperature evolution of lattice constants and volumes, respectively.

is about 1.83 ± 0.41 K, which is smaller than that of Li_2RuO_3 , where the hysteresis loop is about 6 K [11].

At high temperatures, above 125 K, $\chi(T)$ can be fitted very well using a Curie-Weiss behavior $\chi(T) = C/(T - \theta_{CW})$, where C is the Curie constant and θ_{CW} is the Curie-Weiss temperature. The fitted parameters are summarized in Table II. The experimentally obtained effective magnetic moment is slightly larger than the theoretical spin-only value of Ni^{2+} and Mn^{2+} ($\mu_{\text{eff}} = 10.86 \mu_B$) per formula unit, suggesting spin-orbit coupling of Ni moments. In general, the spin component of the effective magnetic moment

of a paramagnet is estimated by the following relation, $\mu_{\text{eff}} = \sum_i g_i [S_i(S_i + 1)]^{1/2}$, where S is the total spin value, with $g_i = 2$, accounting for the contribution of each type of transition metal ion, for Ni^{2+} , $S = 1$ and for Mn^{2+} , $S = 5/2$. There are six Ni^{2+} ions and two Mn^{2+} ions per formula unit. The effective paramagnetic moment per formula unit can be written as $\mu_{\text{eff}} = (4\{6[1(1+1)] + 2[5/2(5/2+1)]\})^{1/2} \mu_B/\text{f.u.} = 10.86 \mu_B/\text{f.u.}$ The fitted Curie-Weiss θ_{CW} show negative values, indicating dominant antiferromagnetic interaction in $\text{PbMn}_2\text{Ni}_6\text{Te}_3\text{O}_{18}$. The estimated values of μ_{eff} and θ_{CW} are in good agreement

TABLE I. The Rietveld refinement result of $\text{PbMn}_2\text{Ni}_6\text{Te}_3\text{O}_{18}$ obtained from room-temperature synchrotron powder x-ray diffraction pattern. The sample adapts the $P6_3/m$ space group (No. 176) with lattice constants $a = 9.28413(8) \text{ \AA}$, $c = 8.81800(9) \text{ \AA}$, and volume $V = 658.24(1) \text{ \AA}^3$, where the goodness of the fits are the weighted profile R factor (Rwp) = 4.83% and goodness of fit (GoF) = 1.63.

Site	x	y	z	Beq/ \AA^{2a}
Pb1	$2b$	0	0	1.81(4)
Mn1	$4f$	$1/3$	$2/3$	0.0590(4)
Ni1	$12i$	0.9885(3)	0.3476(3)	0.9111(2)
Te1	$6h$	0.3623(2)	0.0244(2)	$1/4$
O1	$12i$	0.0978(10)	0.3115(11)	0.0912(10)
O2	$12i$	0.1216(10)	0.6078(11)	0.9147(10)
O3	$6h$	0.4133(18)	0.5531(17)	$1/4$
O4	$6h$	0.2879(16)	0.1889(14)	$1/4$

^aThe isotropic thermal parameters (Beq) of oxygen atoms are constrained to unity for simplification.

with previously reported values for the polycrystalline sample of $\text{PbMn}_2\text{Ni}_6\text{Te}_3\text{O}_{18}$. An empirical value of frustration, $f = |\theta_{\text{CW}}|/T_N$, is found to be around 1.26 ± 0.063 , clearly indicating the absence of strong frustration in $\text{PbMn}_2\text{Ni}_6\text{Te}_3\text{O}_{18}$.

In order to obtain further information about the AFM behavior of $\text{PbMn}_2\text{Ni}_6\text{Te}_3\text{O}_{18}$ we measured the magnetization as a function of magnetic field. Figure 4 shows the magnetization curves at 2 K for fields parallel and perpendicular to the c axis, together with data from a powder sample as a function of magnetic field. The $M(H)$ curves increase linearly with H even up to 7 T, indicating the typical characteristic behavior of an AFM or a paramagnetic (PM) phase. There is no trace of either spin flop or field induced-transitions, or of a saturation of the magnetization curves. The observed magnetic moment at 7 T is smaller than the expected spin-only value ($gS\mu_B$),

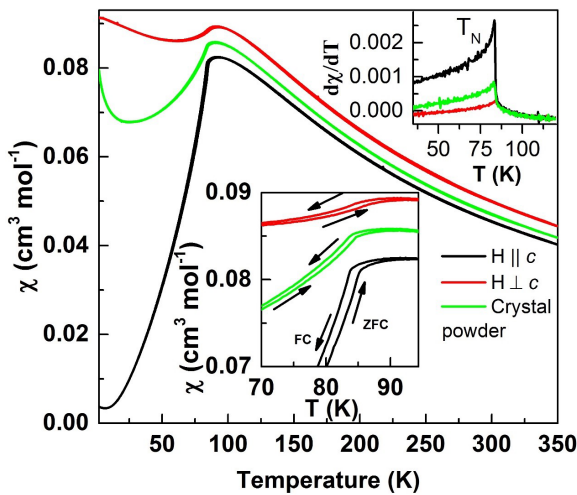


FIG. 3. Magnetic susceptibility versus temperature of $\text{PbMn}_2\text{Ni}_6\text{Te}_3\text{O}_{18}$ measured in a magnetic field of 1 T for a single crystal along different field directions (black and red curves) and for a powder sample (green curve). Upper panel inset: First order derivative of χ . The lower inset shows χ versus temperature around T_N to highlight the behavior near the transition.

TABLE II. Magnetic parameters of $\text{PbMn}_2\text{Ni}_6\text{Te}_3\text{O}_{18}$ single crystals, as Curie constant C , Curie-Weiss θ_{CW} , effective magnetic moment μ_{eff} , and frustration parameter f , extracted from Curie-Weiss law fitting.

Sample	$C(\text{cm}^3 \text{K mol}^{-1})$	$\theta_{\text{CW}}(\text{K})$	$\mu_{\text{eff}}(\mu_B)$	$f = \theta_{\text{CW}} /T_N$
$H \parallel c$	17.19	-107.87	11.73	1.28
$H \perp c$	18.92	-109.73	12.30	1.31
Powder	17.89	-99.96	11.96	1.19

i.e., $7\mu_B/\text{f.u.}$ for $S = 7/2$. This behavior is suggested to be due to the large magnetic field required to achieve an entire spin-only moment. As can be seen in Fig. 5, with increasing magnetic field from 1 to 6 T, T_N does not shift for fields along or perpendicular to the c axis, indicating the AFM-PM phase boundary to be independent of the applied magnetic field ($H \leq 6$ T). It is noteworthy that we have also performed high-temperature magnetic susceptibility experiments between 300 and 800 K with $H \parallel c$ under an applied magnetic field of 1 T as shown in the inset of Fig. 5 (merged with low-temperature susceptibility data). The high-temperature χ data also follow the Curie-Weiss law without any deviation up to 800 K.

To further investigate the AFM long-range order heat capacity [$C_p(T)$] measurements have been performed. $C_p(T)$ for the single crystal in zero magnetic field is depicted in Fig. 6. The $C_p(T)$ value $690 \text{ J mol}^{-1} \text{ K}^{-1}$ at 270 K approaches the Dulong-Petit high-temperature limit of $3NR = 748 \text{ J mol}^{-1} \text{ K}^{-1}$, with the gas constant $R = 8.314 \text{ J mol}^{-1} \text{ K}^{-1}$ and the atomic number $N = 30$. At $T = 85 \text{ K}$, $C_p(T)$ exhibits a distinct λ -type anomaly, which is in good agreement with T_N determined from the derivative of χ . We have also measured $C_p(T)$ upon cooling around T_N , as shown in the upper inset of Fig. 6. There is obviously a small hysteresis between the cooling and warming curves. This is consistent with the thermal hysteresis around T_N observed in our χ measurements.

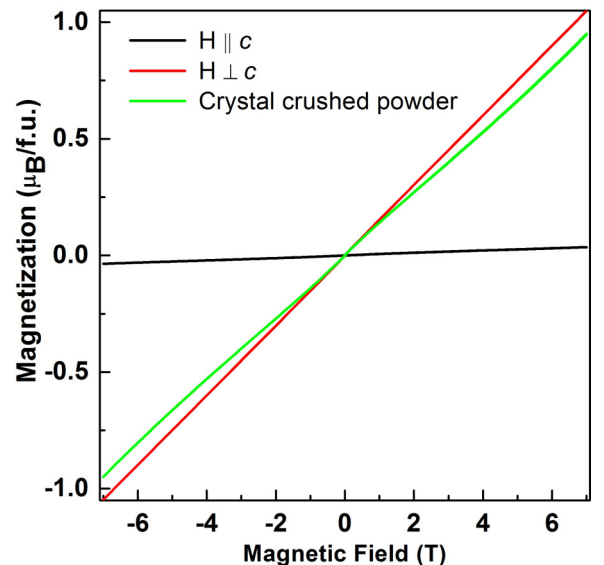


FIG. 4. Field dependence of the magnetization for a single crystal in comparison to powder data of $\text{PbMn}_2\text{Ni}_6\text{Te}_3\text{O}_{18}$.

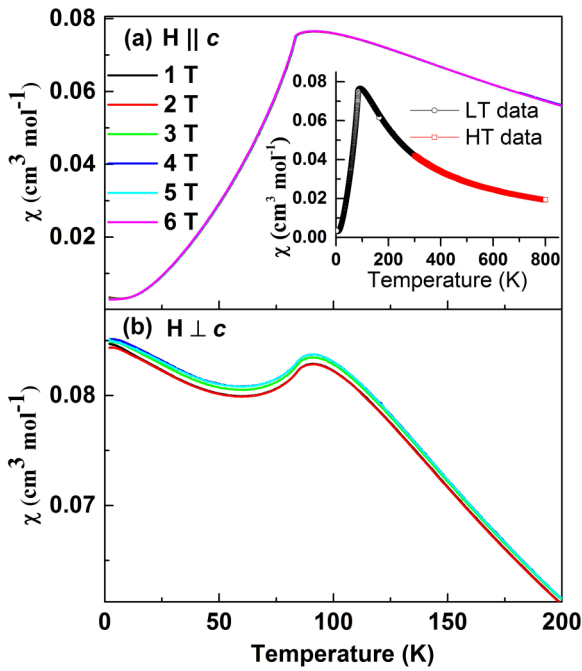


FIG. 5. Temperature dependence of χ at various magnetic fields parallel (a) and perpendicular (b) to the crystallographic c axis. The inset in (a) highlights χ with $H = 1 \text{ T} \parallel c$ for temperatures between 2 and 800 K.

$C_p(T)$ can be well fitted to a conventional Debye T^3 expression considering $C_p(T)/T = \gamma + \beta T^2$ at low temperature, where γ and β are the electronic Sommerfeld specific heat coefficient and lattice specific heat coefficient, respectively. The fit yields $\gamma = 51.03(1) \text{ mJ mol}^{-1} \text{ K}^{-2}$, and $\beta = 6.1(3) \text{ mJ mol}^{-1} \text{ K}^{-4}$. We attribute the nonzero value of γ

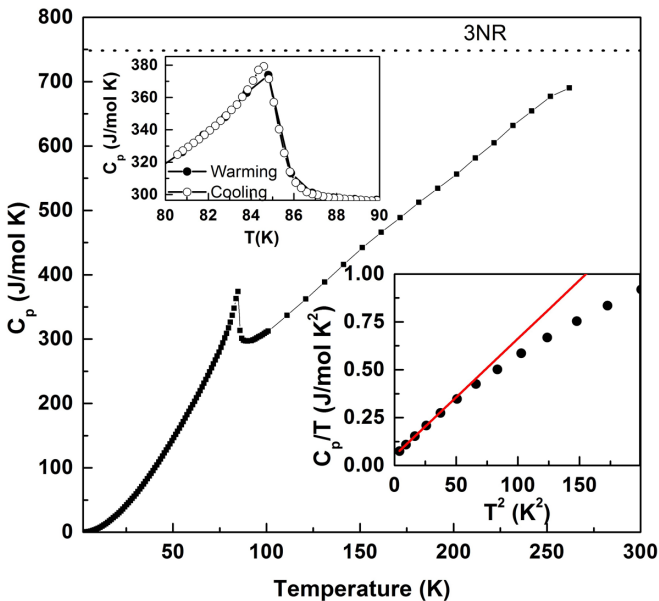


FIG. 6. Specific heat versus temperature for the $\text{PbMn}_2\text{Ni}_6\text{Te}_3\text{O}_{18}$ single crystal in zero magnetic field taken upon heating. Upper inset: C_p data near T_N obtained through cooling and warming. Lower inset: C_p/T versus T^2 at low temperature.

to some glasslike density of states of lattice degrees of freedom, as discussed below. From room temperature transport data we have no evidence of electrical conductivity in $\text{PbMn}_2\text{Ni}_6\text{Te}_3\text{O}_{18}$. Using a Debye model with β value, the Debye temperature, $\Theta = [(12\pi^4 Rn)/(5\beta)]^{1/3}$, is estimated to be 211 K.

$\text{PbMn}_2\text{Ni}_6\text{Te}_3\text{O}_{18}$ consists of a planar network of pairwise rotated NiO_6 dimers coupled by corners. There exist similarities to Ni_3TeO_6 which forms honeycomb layers. The planes in $\text{PbMn}_2\text{Ni}_6\text{Te}_3\text{O}_{18}$ are interstacked with Ni-Te layers in edge-coupled coordinations. This leads to two kinds of channels perpendicular to the layers, one including Mn dimers and the other containing Pb dimers. Therefore we attribute the low-temperature linear specific heat to low-energy structural degrees of freedom due to atomic motions and possible diffusion within the channels. Furthermore, we expect these complex entities (coupled octahedra and planes, as well as dimers) also to show up in structural and magnetic properties.

In our Raman scattering experiments we used a quasibackscattering geometry with the polarization vectors (x and y) within the ab plane. A factor group analysis for the space group $P6_3/m$ with ions residing at the Wyckoff positions detailed in Table I yields a total number of $\Gamma = 21A + 22^2E_2 + 21^1E_1 + 22^1E_2 + 21^2E_1 = 107$ phonons, of which 66 are Raman active [12]. Overall, we investigated 26 modes in detail; see Table III. Due to the needle-shaped samples oriented along the c axis a considerable polarization scrambling is evident and corresponding modes do not show a definite symmetry. They remain without assignment in the table.

In general, phonon modes of $\text{PbMn}_2\text{Ni}_6\text{Te}_3\text{O}_{18}$ are observed in the frequency range $130\text{--}750 \text{ cm}^{-1}$, with the most intense ones at 682 and 700 cm^{-1} . We attribute the generally large Raman scattering intensity in $\text{PbMn}_2\text{Ni}_6\text{Te}_3\text{O}_{18}$ and in particular the intensity of some modes to the involvement of the lone pair element Pb and the TeO_6 group with large electronic polarizability. We have no evidence for a glasslike dynamics of optical phonons. However, such a behavior could be shifted to very low energies and therefore not be observable in our experiments. In Fig. 7(a) we show an overview of Raman spectra in different polarizations. The strong polarization dependence of the intensity points to a pronounced electronic anisotropy. A polarization-independent mode at 299 cm^{-1} might be related to a defect or a surface vibration.

In Table III we show phonon frequencies and tentative assignments, including some references. Modes with frequencies up to 162 cm^{-1} are most probably due to transition metal-Te coordinations. Accordingly, modes in TePb_2 and PbMn are at 162 and 161 cm^{-1} , respectively [13]. The latter group is not represented. Therefore, we conclude it to be TePb_2 . Modes at 206 and 299 cm^{-1} correspond very well to literature values of NiO_6 modes. At higher energies we find excellent agreement with reported data of MnO_6 [13], Ni_3TeO_6 [14], and NiO_6 [15]. The highest-energy modes are fundamental modes of the orthotellurate $(\text{TeO}_6)^{6-}$, that are energetically separated from the conventional lattice modes. Due to this separation these displacements may react like a sensor within the lattice to changes of the electronic and structural environment. Therefore, we have carefully checked the temperature variations of their frequency, linewidth, and intensity.

TABLE III. Phonon frequency, assignment, and reference frequencies of observed phonons in $\text{PbMn}_2\text{Ni}_6\text{Te}_3\text{O}_{18}$ at $T = 5$ K. For some modes corresponding observations exist in Ni_3TeO_6 as reported by Skiadopoulou *et al.* [14]. The strength of the spin-phonon coupling constant λ_{sp} is estimated and noticed as a comment.

Number	Phonon frequency (cm^{-1})	Tentative symmetry	Assignment	Reference frequency	Comment	Reference
1	73	–			Small int.	
2	109	–			Small int.	
3	130	A				
4	141	E_2				
5	147	–				
6	162	A	TePb_2	162		[13]
7	175	E_2				
8	206	E_2	NiO_6	210	Small λ_{sp}	[14]
9	221	A				
10	245	–				
11	299	–	NiO_6	300		[14]
12	359	–	TeO_6	362.2		[14]
13	385	–	TeO_6	385.1		[14]
14	407	E_2	NiO_6	407.1		[15]
15	435	A	TeO_6	430		[14]
16	461	–	TeO_6	470		[14]
17	470	–				
18	509	–	TeO_6	510.3		[14]
19	524	–	MnO_6	522.4		[13]
20	557	–				
21	576	A				
22	605	–				
23	627	A			Large λ_{sp}	
24	682	–	TeO_6	680	Large λ_{sp}	[14]
25	703	–			Small λ_{sp}	
26	752	–				

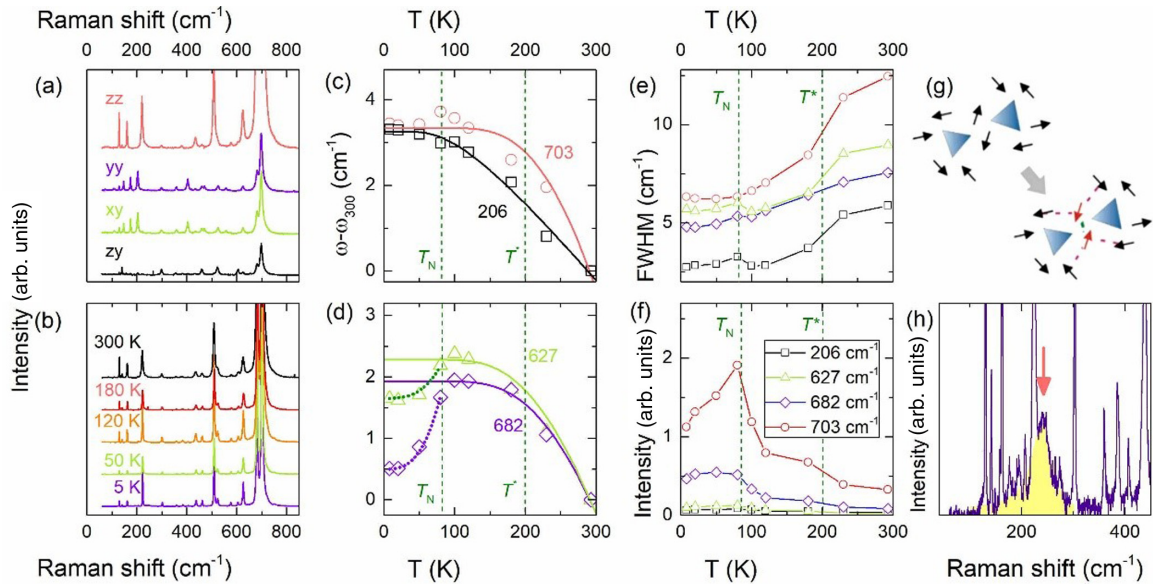


FIG. 7. (a) Raman spectra of $\text{PbMn}_2\text{Ni}_6\text{Te}_3\text{O}_{18}$ in different light polarizations at room temperature. Further details can be found in Table III. (b) Temperature dependence in (xu) polarization. (c), (d) Frequency shift of four selected modes. The solid lines give fits according to a model of anharmonic phonons. (e) Linewidth, and (f) intensity of the modes as a function of temperature. The ordering temperature and a second characteristic temperature T^* are indicated by dashed lines. (g) Sketch of a spin exchange process. The dashed lines correspond to the modified spin configuration by exchange. This geometry leads to a coordination number of $z = 3$ of each spin. (h) Continuum of scattering with a maximum at 240 cm^{-1} that is a candidate for two-magnon scattering.

The temperature dependencies of selected phonon frequencies, linewidths, and intensities are plotted in Figs. 7(c)–7(f). These temperature dependencies can be described by a superposition of phonon anharmonicities, i.e., a decay into acoustic phonons, and a coupling to the spin system evident at $T_N = 84$ K, as well as another, unique effect at $T^* \approx 200$ K.

Phonon anharmonicities may be described in a simple framework considering occupied states with Bose statistics by fitting the data to the following equation, $\omega_{\text{ph}}(T) = \omega_0 + C\{1 + 2/[\exp(\hbar\omega_0/k_B T) - 1]\}$, with ω_{ph} , ω_0 , and C , the experimental frequency, the unrenormalized frequency, and a constant, respectively. This leads to a good description of the data in Fig. 7(c).

However, phonon frequencies in panel (d) deviate rather strongly for $T < T_N$. Such anomalies are related to the onset of long-range order at $T_N = 84$ K, and indicate that the respective displacements modulate the spin exchange interaction. As a consequence, the spin system of $\text{PbMn}_2\text{Ni}_6\text{Te}_3\text{O}_{18}$ decreases the energy of the lattice system. The resulting phonon shift is given by the first moment of the spin-spin correlation function, i.e., $\omega_{\text{ph}}/\omega_0 \propto \lambda_{\text{sp}}\langle\text{SS}\rangle$, with the spin-phonon coupling constant $\lambda_{\text{sp}}(k \rightarrow 0)$ in the limit of small momenta. This correlation function is proportional to the change of the magnetic moment with temperature $[\Delta m(T)]$. From the difference of the anharmonic fit to the observed data this correlation function can be derived, $\langle\text{SS}\rangle \propto -\Delta m(T)/m_0$, where m_0 is the magnetic moment at $T = 0$. Here it fits rather well to a mean-field expression $\Delta\omega/\omega = 1 - (T/T_N)^2$. In Table III modes with particularly large λ_{sp} are assigned.

The phonon linewidths and the phonon intensities show anomalies related to anharmonicity as well. For all modes the linewidth decreases with decreasing temperature. However, the modes have a rather different linewidth in the limit $T \rightarrow 0$. High-frequency modes have the largest linewidth and they show the largest anomaly of intensity at $T_N = 84$ K. This points to the fact that these modes couple efficiently to spin fluctuations. The mode at 206 cm^{-1} related to NiO_6 can be taken as a reference as it is a rather conventional lattice vibration with small spin-phonon coupling.

It is noteworthy that the linewidth and intensity in Figs. 7(e) and 7(f) also show anomalies at the characteristic temperature $T^* \approx 200$ K, similar to the ones at $T_N = 84$ K. This gives evidence for some instability of the spin/lattice system that is often observed in oxides with highly polarizable ions. Modes with the largest spin-phonon related anomalies at $T_N = 84$ K are not identical with modes that show the largest effects at $T^* \approx 200$ K. Therefore, these effects at the two characteristic temperatures are dissimilar. This difference exists despite their very similar frequencies related to the displacements of the orthotellurate $(\text{TeO}_6)^{6-}$. Therefore, we attribute the spin-phonon anomalies to a binding to NiO_6 and the anomalies at $T^* \approx 200$ K to a proximity of the lone pair ion Pb^{2+} to the tellurate.

At approximately 240 cm^{-1} we identify a candidate for magnetic Raman scattering as a broad and spiked maximum with a linewidth of 100 cm^{-1} . In Figs. 7(g) and 7(h) this continuum is shown together with a sketch of the exchange process. Within an Ising picture of light-induced spin exchange in an antiferromagnetically coordinated spin network Raman scattering corresponds to breaking exchange bonds.

The number of broken bonds in a certain exchange geometry gives an estimate of the characteristic energy of two-magnon Raman scattering. In $\text{PbMn}_2\text{Ni}_6\text{Te}_3\text{O}_{18}$ there are two different magnetic ions at multiple crystallographic sites. The larger number of Ni ions and their closer coordination in a triangular plane motivates us to restrict ourselves to these sites as contributors for magnetic Raman scattering. As an approximation this leads to $J = -E_{\text{max}}/2S(z-1)$, where E_{max} corresponds to the energy of the maximum Raman intensity of the two-magnon scattering; with $S = 1$, the coordination number $z = 3$, and $E_{\text{max}} = 345$ K, a coupling strength of $J = -86$ K is resolved. This exchange magnitude fits reasonably well to the Curie-Weiss constant of approximately -110 K determined from the magnetic susceptibility considering that only the coordinations of the Ni are taken into account.

IV. CONCLUSION

We have grown single crystals of $\text{PbMn}_2\text{Ni}_6\text{Te}_3\text{O}_{18}$ and have studied their structural, magnetic, and thermal properties. This compound orders antiferromagnetically below about ~ 84 K, which is most likely a first order transition, as hysteretic behavior is observed around the AFM transition. From the low-temperature Debye model, the Debye temperature for $\text{PbMn}_2\text{Ni}_6\text{Te}_3\text{O}_{18}$ is determined to be 211 K. We have investigated 26 phonon modes as a part of the Raman as well as IR active total number of $\Gamma = 21A + 22^2E_2 + 21^1E_1 + 22^1E_2 + 21^2E_1 = 107$ phonons. Our analysis of the temperature dependence of Raman scattering spectra showed that the observed effects, such as phonon frequencies, linewidths, and intensities, are due to a superposition of phonon anharmonicities, a coupling to the spin system evident at $T_N = 84$ K, as well as another, unique effect at $T^* \approx 200$ K. The phonon linewidths and intensities behave similarly to those at $T_N = 84$ K. Raman spectra also revealed the existence of two-magnon excitations, from which an exchange coupling strength $J = -86$ K is estimated.

ACKNOWLEDGMENTS

I.P.M. thanks the Department of Science and Technology in India for the support of INSPIRE Faculty Award No. DST/INSPIRE/04/2016/002275 (IFA16-PH171). K.S. acknowledges the financial assistance from University Grants Commission, India for D. S. Kothari Postdoctoral Fellowship (DSKPDF) Award No. F.4-2/2006 (BSR)/PH/18-19/0099. P.L. acknowledges support by Deutsche Forschungsgemeinschaft (DFG, German Research Foundation) Grants No. DFG LE967/16-1 and No. DFG EXC-2123 Quantum Frontiers 390837967. D.W. acknowledges support by the Institute for Basic Science (Grant No. IBS-R009-Y3), “Niedersächsisches Vorab” through “Quantum-, and Nano-Metrology (QUANOMET), NL-4.” R.S. acknowledges financial support provided by the Ministry of Science and Technology in Taiwan under Projects No. MOST-108-2112-M-001-049-MY2 and No. MOST 109-2124-M-002-001, and Sinica funded i-MATE Financial Support No. AS-iMATE-109-13.

- [1] F. D. M. Haldane, *Phys. Lett. A* **93**, 464 (1983).
- [2] F. D. M. Haldane, *Phys. Rev. Lett.* **50**, 1153 (1983).
- [3] W. J. L. Buyers, R. M. Morra, R. L. Armstrong, M. J. Hogan, P. Gerlach, and K. Hirakawa, *Phys. Rev. Lett.* **56**, 371 (1986).
- [4] R. M. Morra, W. J. L. Buyers, R. L. Armstrong, and K. Hirakawa, *Phys. Rev. B* **38**, 543 (1988).
- [5] J. F. DiTusa, S.-W. Cheong, J.-H. Park, G. Aeppli, C. Broholm, and C. T. Chen, *Phys. Rev. Lett.* **73**, 1857 (1994).
- [6] A. Zheludev, J. M. Tranquada, T. Vogt, and D. J. Buttrey, *Phys. Rev. B* **54**, 6437 (1996).
- [7] A. Zheludev, J. M. Tranquada, T. Vogt, and D. J. Buttrey, *Phys. Rev. B* **54**, 7210 (1996).
- [8] B. Wedel, K. Sugiyama, K. Hiraga, and K. Itagaki, *Mater. Res. Bull.* **34**, 2193 (1999).
- [9] Y. Doi, R. Suzuki, Y. Hinatsu, K. Kodama, and N. Igawa, *Inorg. Chem.* **54**, 10725 (2015).
- [10] I. P. Muthuselvam, R. Sankar, A. V. Ushakov, W. T. Chen, G. Narsinga Rao, S. V. Streltsov, S. K. Karna, L. Zhao, M. K. Wu, and F. C. Chou, *J. Phys.: Condens. Matter* **27**, 456001 (2015).
- [11] K. Mehlawat and Y. Singh, *Phys. Rev. B* **95**, 075105 (2017).
- [12] <http://www.crust.ehu.es/rep/sam.html>.
- [13] J. Weidlein, U. Müller, and K. Dehnicke, *Schwingungsfrequenzen I* (Georg Thieme Verlag, Stuttgart, 1981); *Schwingungsfrequenzen II* (Georg Thieme Verlag, Stuttgart, 1986).
- [14] S. Skiadopoulou, F. Borodavka, C. Kadlec, F. Kadlec, M. Retuerto, Z. Deng, M. Greenblatt, and S. Kamba, *Phys. Rev. B* **95**, 184435 (2017).
- [15] G. Gou, I. Grinberg, A. M. Rappe, and J. M. Rondinelli, *Phys. Rev. B* **84**, 144101 (2011).